

Understanding the Characteristics of Multiple Production of Light Hadrons in $Cu + Cu$ Interactions at Various RHIC Energies: A Model-based Analysis

P. Guptaroy^{1*}, Goutam Sau^{2†}, S. K. Biswas³ & S. Bhattacharyya^{4‡}

¹ Department of Physics, Raghunathpur College,
P.O.: Raghunathpur 723133, Dist.: Purulia(WB), India.

² Beramara Ram Chandrapur High School,
South 24-Parganas, 743609(WB), India.

³ West Kodalia Adarsha Siksha Sadan, New Barrackpore,
Kolkata-700131, India.

⁴ Physics and Applied Mathematics Unit(PAMU),
Indian Statistical Institute,
203 B. T. Road, Kolkata - 700108, India.

Abstract

Experiments involving copper-copper collisions at the RHIC-BNL (USA) at energies $\sqrt{s_{NN}} = 22.5, 62$ and 200 GeV have produced a vast amount of high-precision data which are to be analysed in the light of various competing models in the domain of multiparticle production scenario. We have chosen to analyse here the measured data on the p_T -spectra of various light and non-strange secondaries at various energies mentioned above, some of their very important ratio-behaviours at the various centralities of the collisions and the nuclear modification factors, R_{AA} and R_{CP} , in the light of a version of the Sequential Chain Model (SCM). The agreements between the measured data and model-based results are generally found to be modestly satisfactory. Besides, our obtained results have also been compared with results based upon two approaches with strong standard model flavour, of which one is purely pQCD-oriented and is forwarded by Vitev.

Keywords: Relativistic heavy ion collisions, inclusive production, quark gluon plasma
PACS nos.: 25.75.q, 13.85.Ni, 12.38.Mh

*e-mail: gpradeepta@rediffmail.com

†e-mail: gautamsau@yahoo.co.in

‡e-mail: bsubrata@isical.ac.in (Communicating Author).

1 Introduction

In a previous paper [1] we dealt with the properties of $Au + Au$ interactions at RHIC-energies at $\sqrt{s_{NN}}=200$ GeV in great detail with emphasis on the nature of the most important observables. The gold-gold interactions constituted a relatively heavy system. Compared to it, the $Cu + Cu$ system represents a lighter and smaller system-size, with mass-number for copper being much less than gold. Besides, in Ref. [1] we also gave the details about the essential points of the basic multiparticle production model applied therein.

So, in order to avoid repetitions, we will just give a very brief sketch of the main/major observables that would here be dealt with and on the same model that we make use of here.

Our purpose is to check (i) whether the same model could explain the data measured for a comparatively lighter system; (ii) whether [and to what extent (if at all)] there is any prominent system size effect on the results obtained by the experimental measurements.

Apart from the nature of p_T -spectra and some particle-production ratios, we will dwell upon here properties of nuclear modification factors R_{AA} and R_{CP} for $Cu + Cu$ collisions and the centrality dependence of the results. But production of the heavies and the heavy strange hadrons are left out in the present work.

As our approach to the analysis of $Cu + Cu$ collisions (or for that matter, of $Au + Au$ and even $p + p$ reactions) is somewhat different from the ‘standard’ varieties, our phrases and vocabularies are not identical with them. We have inducted here the physics of partonic multiple scatterings for both nucleus-nucleus interactions, and $p + p$ reactions at large- p_T through some mechanism as given in the text in the appropriate place. Even the effects of rescatterings have also been incorporated here by the same technique. But, the associated hadronic collectivity factor (gauged by the elliptic flow represented normally by ‘ v_2 ’) has not been touched upon here; this flow-behaviour would be dwelt-upon in some detail in a future work.

In order to dispel any misunderstanding of any interested reader, let us emphasise here, before closing up the introductory remarks, that our intention is not to make any tall claim that the model tried out and tested here is much better than the existing models. But, our objective is just to familiarise the fact that modest description of data is quite possible even with some non-standard approaches, like the present one, which is being applied and validated to explain some observables in high energy collisions since the mid-seventies.

Finally, the organization of this work is as follows. In section 2 we sum up the main physics-aspects entailed in this work. A glance and a glimpse into it would reveal the non-standard

nature of the basic approach. In the next section (section 3) the results arrived at have been presented with tables and figures. The section 4 provides some comparison of our work with both data and the results obtained by other model-based approaches for a very few observables related to the production of some very select secondaries (for which theory-based studies on $Cu + Cu$ collisions are available). And in the last section (section 5) we offer the final comments and conclusions.

2 The Theoretical Framework: A Brief Outlook

The description of the model-based features would be subdivided into some parts. The first part (subsection 2.1) gives a brief overview of the production mechanism of the secondary hadrons in nucleon-nucleon ($p+p$) interaction in the context of the Sequential Chain Model (SCM). Then in the subsection 2.2 we present a brief outline of the main and major achievements of the model; these points, in essence, also highlight the important characteristics of the model. Thereafter, the relevant transitions for different observables from $p+p$ to $A+B$ interactions will be discussed in the subsection 2.3.

2.1 Basic Model for Particle Production in PP Scatterings: An Outline

According to this Sequential Chain Model (SCM), high energy hadronic interactions boil down, essentially, to the pion-pion interactions; as the protons and neutrons are conceived in this model as $p = (\pi^+ \pi^0 \vartheta)$ and $n = (1/\sqrt{\chi_1^2 + \chi_2^2} [\chi_1(\pi^0 \pi^0 \vartheta) + \chi_2(\pi^- \pi^+ \vartheta)])$ respectively, where ϑ is a spectator particle needed for the dynamical generation of quantum numbers of the nucleons and χ_1, χ_2 are the weightage factors [1]-[5]. Our focus and concern would now be confined and concentrated to the structure of protons alone. The production of pions in the present scheme occurs as follows: the incident energetic π -mesons in the structure of the projectile proton(nucleon) emits a rho(ρ)-meson in the interacting field of the pion lying in the structure of the target proton, the ρ -meson then emits a π -meson and is changed into an omega(ω)-meson, the ω -meson then again emits a π -meson and is transformed once again into a ρ -meson and thus the process of production of pion-secondaries continue in the sequential chain of ρ - ω - π mesons. The two ends of the diagram contain the baryons exclusively [1]-[5].

For $K^+(K^-)$ or $K^0\bar{K}^0$ production the model proposes the following mechanism. One of the interacting π -mesons emits a ρ -mesons; the ρ -mesons in its turn emits a ϕ^0 -meson and a π -meson.

The π -meson so produced then again emits ϱ and ϕ^0 mesons and the process continues. The ϕ^0 mesons so produced now decays into either K^+K^- or $K^0\bar{K}^0$ pairs. The ϱ - π chain proceeds in any Feynmann diagram in a line with alternate positions, pushing the ϕ^0 mesons (as producers of K^+K^- or $K^0\bar{K}^0$ pairs) on the sides. This may appear paradoxical as the ϕ^0 production cross-section is generally smaller than the $K\bar{K}$ production cross-section; still the situation arises due to the fact that the ϕ^0 resonances produced in the collision processes will quickly decay into $K\bar{K}$ pairs, for which the number of ϕ^0 will be lower than that of the $K\bar{K}$ pairs. Besides, as long as ϕ^0 mesons remain in the virtual state, theoretically there is no problem, for $\phi^0 K^+K^-$ (or $\phi^0 K^0\bar{K}^0$) is an observed and allowed decay mode, wherein the strangeness conservation is maintained with the strange-antistrange coupled production. Moreover, $\phi^0 K^+K^-$ (or $\phi^0 K^0\bar{K}^0$) coupling constant is well known and is measured by experiments with a modest degree of reliability. And we have made use of this measured coupling strength for our calculational purposes, whenever necessary. It is assumed that the K^+K^- and $K^0\bar{K}^0$ pairs are produced in equal proportions [1]-[5]. The entire production process of kaon-antikaons is controlled jointly by the coupling constants, involving ϱ - π - ϕ and ϕ^0 - K^+K^- or ϕ^0 - $K^0\bar{K}^0$.

Now we describe here the baryon-antibaryon production. According to the SCM mechanism, the decay of the pion secondaries produces baryon-antibaryon pairs in a sequential chain as before. The pions producing baryons-antibaryons pairs are obviously turned into the virtual states. And the proton-antiproton pairs are just a part of these secondary baryon-antibaryon pairs. In the case of baryon-antibaryon pairs it is postulated that protons-antiprotons and neutrons-antineutrons constitute the major bulk, Production of the strange baryons-antibaryons are far less due to the much smaller values of the coupling constants and due to their being much heavier.

The field theoretical calculations for the average multiplicities of the π , K and \bar{p} -secondaries and for the inclusive cross-sections of those secondary particles deliver some expressions which we would pick up from [1]-[5].

The inclusive cross-section of the π^- -meson produced in the $p + p$ collisions given by

$$E \frac{d^3\sigma}{dp^3} \Big|_{pp \rightarrow \pi^- x} \cong \Gamma_{\pi^-} \exp(-2.38 \langle n_{\pi^-} \rangle_{pp} x) \frac{1}{p_T^{(N_R^-)}} \exp\left(\frac{-2.68 p_T^2}{\langle n_{\pi^-} \rangle_{pp} (1-x)}\right), \quad (1)$$

with

$$\langle n_{\pi^+} \rangle_{pp} \cong \langle n_{\pi^-} \rangle_{pp} \cong \langle n_{\pi^0} \rangle_{pp} \cong 1.1s^{1/5}, \quad (2)$$

where Γ_{π^-} is the normalisation factor which will increase as the inelastic cross-section increases

and it is different for different energy region and for various collisions, for example, $|\Gamma_{\pi^-}| \cong 90$ for Intersecting Storage Ring(ISR) energy region. The terms p_T , x in equation (1) represent the transverse momentum, Feynman Scaling variable respectively. Moreover, by definition, $x = 2p_L/\sqrt{s}$ where p_L is the longitudinal momentum of the particle. The s in equation (2) is the square of the c.m. energy.

$1/p_T^{N_R^{\pi^-}}$ of the expression (1) is the ‘constituent rearrangement term’ arising out of the partons inside the proton which essentially provides a damping term in terms of a power-law in p_T with an exponent of varying values depending on both the collision process and the specific p_T -range. The choice of N_R would depend on the following factors: (i) the specificities of the interacting projectile and target, (ii) the particularities of the secondaries emitted from a specific hadronic or nuclear interaction and (iii) the magnitudes of the momentum transfers and of a phase factor (with a maximum value of unity) in the rearrangement process in any collision. And this is a factor for which we shall have to parameterize alongwith some physics-based points indicated earlier. The parametrization is to be done for two physical points, viz., the amount of momentum transfer and the contributions from a phase factor arising out of the rearrangement of the constituent partons. Collecting and combining all these, we proposed the relation to be given by [6]

$$N_R = 4 \langle N_{part} \rangle^{1/3} \theta, \quad (3)$$

where $\langle N_{part} \rangle$ denotes the average number of participating nucleons and θ values are to be obtained phenomenologically from the fits to the data-points. In this context, the only additional physical information obtained from the observations made here is: with increase in the peripherality of the collisions the values of θ gradually grow less and less, and vice versa.

Similarly, for kaons of any specific variety (K^+ , K^- , K^0 or \bar{K}^0) we have

$$E \frac{d^3\sigma}{dp^3} |_{pp \rightarrow K^-x} \cong \Gamma_{K^-} \exp(-6.55 \langle n_{K^-} \rangle_{pp} x) \frac{1}{p_T^{(N_R^{K^-})}} \exp\left(\frac{-1.33 p_T^2}{\langle n_{K^-} \rangle_{pp}^{3/2}}\right), \quad (4)$$

with $|\Gamma_{K^-}| \cong 11.22$ for ISR energies and with

$$\langle n_{K^+} \rangle_{pp} \cong \langle n_{K^-} \rangle_{pp} \cong \langle n_{K^0} \rangle_{pp} \cong \langle n_{\bar{K}^0} \rangle_{pp} \cong 5 \times 10^{-2} s^{1/4}. \quad (5)$$

And for the antiproton production in pp scattering at high energies, the derived expression for inclusive cross-section is

$$E \frac{d^3\sigma}{dp^3} \Big|_{pp \rightarrow \bar{p}x} \cong \Gamma_{\bar{p}} \exp(-25.4 \langle n_{\bar{p}} \rangle_{pp} x) \frac{1}{p_T^{(NR\bar{p})}} \exp\left(\frac{-0.66((p_T^2)_{\bar{p}} + m_{\bar{p}}^2)}{\langle n_{\bar{p}} \rangle_{pp}^{3/2} (1-x)}\right), \quad (6)$$

with $|\Gamma_{\bar{p}}| \cong 1.87 \times 10^3$ and $m_{\bar{p}}$ is the mass of the antiprotons. For ultrahigh energies

$$\langle n_{\bar{p}} \rangle_{pp} \cong \langle n_p \rangle_{pp} \cong 2 \times 10^{-2} s^{1/4}, \quad (7)$$

2.2 Some Cardinal Characteristics and Triumphs of the Model

We agree that the word ‘non-standard’ used in the preceding section is a *port manteau* adjective, with many layers of meaning hidden within it. In this particular case, (i) the model is based on some new ideas about the structure of hadrons and the nature of hadronic interactions; (ii) the proposed mechanism underlying this work does not admit of any airtight compartmentalisation of the ‘soft’ (low- p_T) and ‘hard’(large p_T , $p_T \geq 2$ GeV/c) production; (iii) rather, the model presents a unified approach to the production of particle-secondaries; (iv) besides, the fundamental expressions for final (analytical) calculations are derived here on the basis of field-theoretic considerations and the use of Feynman diagram techniques (albeit with some simplifying high energy approximation and assumptions) with the infinite momentum frame tools and under impulse approximation method; (v) this approach establishes the \langle *universality* \rangle aspect of the multiplicity of high energy interaction called ‘globality property’; (vi) the model explains the ‘jet’-structure for emanation of the secondary particle as the $\langle\langle$ *two – sidedsprays* $\rangle\rangle$ of hadrons, (vii) it reproduces the behaviour of average multiplicity, nature of (invariant) inclusive cross-section and the properties of average transverse momenta of various secondaries; (viii) the model could also account for the very slow rising nature of the total cross-sections. (ix) Besides, this model can/does explain the majority of the characteristics of what are known or believed to be the ‘quark gluon plasma’-diagnostics. And that could be obviously done by an alternative approach and outlook. (x) Furthermore, the application of the model can also accommodate a large amount of very important Cosmic Ray Physics issues and problems that came to the fore in the very recent times.

The above-mentioned features are essentially ingrained in the entirety of this totally non-standard mechanism emerging from an alternative philosophy and outlook about the particle-constituents and their interaction mode. On the whole, this is purely an analytical approach with a reasonable number of valid assumptions and approximations which are commonly used by all High Energy Physicists. Uptil now, we have confined ourselves mostly to the non-simulational

calculations. The calculations for ‘soft’ and ‘hard’ have been superposed here by virtue of the simple factorisation property. One of the very strong points about this model is the fact that the various coupling strengths used in this model are not only known but also reliably well-measured by several experiments. This factor helps to reduce considerably the speculative components in the results.

2.3 Results for AA Collisions from PP Reactions: The Connecting Bridge

In order to study a nuclear interaction of the type $A+B \rightarrow C^- + x$, where A and B are projectile and target nucleus respectively, and C^- is the detected particle which, in the present case, would be π^- , K^- and \bar{p} , the SCM has been adapted, on the basis of the suggested Wong [7] work to the Glauber techniques by using Wood-Saxon distributions [8]-[9]. The details of calculations and the features of the SCM have been given in our previous paper [1].

The general form of our SCM-based transverse-momentum distributions for $A+B \rightarrow C^- + X$ -type reactions can be written in the following notation:

$$\frac{1}{2\pi p_T} \frac{d^2 N}{dp_T dy} |_{A+B \rightarrow C^- + x} = \alpha_{C^-} \frac{1}{p_T^{N_{R}^{C^-}}} \exp(-\beta_{C^-} \times p_T^2). \quad (8)$$

The set of relations to be used for estimating the parameter α_{C^-} is given below [1].

$$\alpha_{C^-} = \frac{(A\sigma_B + B\sigma_A)}{\sigma_{AB}} \frac{1}{1 + a(A^{1/3} + B^{1/3})} \Gamma_{C^-} \exp(-\eta < n_{C^-} >_{pp} x) \quad (9)$$

Here, in the above equation [eqn.(9)], Γ_{C^-} , as stated above, is the normalization constant which is different for the different secondaries and the collider energies. It also depends on the centrality of the collisions. The first factor in eqn.(9) gives a measure of the number of wounded nucleons i.e. of the probable number of participants, wherein $A\sigma_B$ gives the probability cross-section of collision with ‘ B ’ nucleus (target), had all the nucleons of A suffered collisions with B -target. And $B\sigma_A$ has just the same physical meaning, with A and B replaced. Furthermore, σ_A is the nucleon(proton)-nucleus(A) interaction cross-section, σ_B is the inelastic nucleon(proton)-nucleus(B) reaction cross-section and σ_{AB} is the inelastic AB cross-section for the collision of nucleus A and nucleus B . The values of σ_{AB} , σ_A , σ_B are worked here out in a somewhat heuristic manner by the following formula [10]

$$\sigma_{AB}^{inel} = \sigma_0 (A_{projectile}^{1/3} + A_{target}^{1/3} - \delta)^2 \quad (10)$$

with $\sigma_0 = 68.8$ mb, $\delta = 1.32$.

Besides, in expression (9), the second term is a physical factor related with energy degradation of the secondaries due to multiple collision effects. The parameter a occurring in eqn.(9) above is a measure of the fraction of the nucleons that suffer energy loss. The maximum value of a is unity, while all the nucleons suffer energy loss. This a parameter is usually to be chosen [7], depending on the centrality of the collisions and the nature of the secondaries.

The values of η in eqn. (9) are different for different secondary produced; for example, $\eta=2.38$ for pions, 6.35 for kaons and 25.4 for protons, as were given in eqn.(1), eqn.(4) and eqn.(6).

$1/p_T^{N_C^-}$ of the expression (8) is the ‘constituent rearrangement term’ arising out of the partons inside the proton which essentially provides a damping term in terms of a power-law in p_T with an exponent of varying values depending on both the collision process and the specific p_T -range. We have already mentioned the details earlier.

The values of β_{C^-} of the equation (8) for different secondaries have been calculated with the help of eqn.(1), eqn.(2), eqn.(4)-eqn.(7).

3 Steps Towards Calculations

At the very start let us present a summary (which might be a rehash of what we have mentioned) of the key physical facts that would be of paramount importance which proceeding towards calculations. There are some foundational steps that enable us to arrive at the final working formulae which deliver the results to be reported here for for $Cu + Cu$ collisions. The procedural steps are as follows: (i) Firstly, we have the basic model for $p + p$ scattering at high energies and low- p_T (‘soft’) interactions, so we have to convert the mathematical expressions for nucleus+nucleus ($Cu + Cu$) collisions by introducing the nuclear dependence factor on the results arrived at for $p + p$ collisions. (ii) Secondly, the data-points on $Cu + Cu$ reaction at various high energies exceed the range of the low- p_T boundary, $p_T > 2$ GeV/c, for which the large- p_T effect is to be superposed on the expressions for soft-production of the secondaries. The constituent(partonic) rearrangement factor introduced here takes care of this physical feature arising out of the ‘hard’ (large- p_T) contributions. (iii) In a model-dependent way the SCM has some special and specific means of excess production of the positive secondaries, specifically the light secondaries.

Table 1: Values of $(\alpha_{\pi^-})_{pp}$, $(N_R^{\pi^-})_{pp}$ and $(\beta_{\pi^-})_{pp}$ for π^- productions in $p + p$ collisions at $\sqrt{s_{NN}}=20, 63$ and 200 GeV

$\sqrt{s_{NN}}$	$(\alpha_{\pi^-})_{pp}$	$(N_R^{\pi^-})_{pp}$	$(\beta_{\pi^-})_{pp}$
20 GeV	0.281	4.086	0.703
63 GeV	0.545	3.327	0.468
200 GeV	0.007	3.867	0.293

3.1 Production of Main Varieties of Negatively Charged Secondaries

The general expressions of inclusive cross-sections for the production of π^- , K^- and \bar{p} for $p + p$ collisions were stated in the previous section by eqn.(1), eqn.(4) and eqn.(6) respectively.

For the production of π^- -mesons in $p + p$ collisions, we use eqn.(1), eqn.(2) and eqn.(9) with $\alpha_{\pi^-} = \Gamma_{\pi^-} \exp(-2.38 < n_{\pi^-} >_{pp} x)$. The values of $(\alpha_{\pi^-})_{pp}$, $(N_R^{\pi^-})_{pp}$ and $(\beta_{\pi^-})_{pp}$ are given in Table 1. The experimental data for the inclusive cross-sections versus $p_T[GeV/c]$ for π^0 production in $p + p$ interactions at $\sqrt{s_{NN}} = 20$ GeV are taken from Ref. [12]. And for the data for inclusive cross-sections for π^+ at energies $\sqrt{s_{NN}} = 63$ GeV and $\sqrt{s_{NN}} = 200$ GeV we use references [13], [14], [15] respectively. They are plotted in Figure 1(a), Figure 1(b) and Figure 1(c) respectively. The solid lines in those figures depict the SCM-based plots.

3.1.1 Production of π^- -mesons in $Cu + Cu$ Collisions

We now, at first, turn our attention to π^- production in $Cu + Cu$ collisions at energies $\sqrt{s_{NN}} = 22.5, 62.4$ and 200 GeV.

Using eqn.(8) and eqn.(9) the SCM-based expressions for transverse momentum distribution of negative pions produced in the $Cu + Cu$ collisions at $\sqrt{s_{NN}} = 22.5, 62.4$ and 200 GeV at RHIC and for different centralities can be obtained. The values of α_{π^-} , $N_R^{\pi^-}$ and β_{π^-} for different centralities and for different energies are given in Table 2. The values of N_{part} , for calculating $N_R^{\pi^-}$ from eqn.(3), in this context, have been taken from Ref. [16], [17]. The experimental results for the production of π^- at different centralities for energies $\sqrt{s_{NN}} = 22.5, 62.4$ GeV are taken from the Ref. [18] and for energy $\sqrt{s_{NN}} = 200$ GeV we have used Ref. [19]. The invariant yields for π^- against $p_T[GeV/c]$ for different energies are plotted in Figures 2(a), 2(b) and 2(c) respectively. The solid lines in those figures show the theoretical SCM results.

3.1.2 K^- Production in $Cu + Cu$ Collisions

With the help of the eqn.(3)-eqn. (5), eqn. (8) and eqn. (9) the values of α_{K^-} , $N_R^{K^-}$ and β_{K^-} for the transverse momentum distributions for different centralities of K^- -particles in $Cu + Cu$ collisions at $\sqrt{s_{NN}} = 22.5, 62.4$ and 200 GeV at RHIC have been calculated and they are given in Table 3. The experimental results are taken from the PHENIX group[18] for RHIC energies $\sqrt{s_{NN}} = 22.5$ and 62.4 GeV and they are plotted in Figures 4(a) and 4(b), whereas for $\sqrt{s_{NN}} = 200$ GeV, the Ref. [19] has been used and data are plotted in Fig. 4(c). The lines in those figures depict the theoretical outcomes.

3.1.3 Production of \bar{p} in $Cu + Cu$ Collisions at Different Energies

Using the eqn.(6)-eqn.(9), the transverse momentum distributions for antiproton in $Cu + Cu$ collisions at energies $\sqrt{s_{NN}} = 22.5, 62.4$ and 200 GeV at RHIC have been calculated the corresponding values of $\alpha_{\bar{p}}$, $N_R^{\bar{p}}$ and $\beta_{\bar{p}}$ for different centralities and different energies are given in Table 4. The experimental results of invariant yields for the production of antiproton productions for energies $\sqrt{s_{NN}} = 22.5, 62.4$ GeV and for $\sqrt{s_{NN}} = 200$ GeV are taken from the Refs. [18], [19] respectively. They are plotted against p_T in Figures 6(a), 6(b) and 6(c) for different centralities. The solid lines in those figures show the theoretical SCM-based results.

3.2 On Excess Production of Positive Particles

True, on the average, the particles are produced in charge-independent equal measure, for which roughly one-third of the particles could be reckoned to be positively charged, one third are negatively charged and the rest one third are neutral. But, according to the present mechanism of particle production, there are some specifically exclusive means to produce positive particles of which π^+ , K^+ , and p are the members. They are produced from within the structure of protons (nucleons). These production characteristics and the quantitative expressions for their special production have been dwelt upon in detail in Ref. [5]. Let us assort the relevant expressions therefrom as results to be used here.

3.2.1 Production of Positive Pions in $Cu + Cu$ Collisions

For production of positive pions [π^+ mesons] the excess term could be laid down by the following expressions [5]:

$$(B_{\pi^+})_{pp} = \frac{4}{3} g_{p\pi\pi}^2 \frac{(P' + K)^2}{[(P' + K)^2 - m_p^2]^2} A(\nu, q^2)_\pi \int \frac{d^3 k_\pi}{2k_0(2\pi)^3} \exp(-ik_\pi x), \quad (11)$$

where the symbols have their contextual connotation with the following hints to the physical reality of extraneous π^+ , as non-leading secondaries. The first parts of the above equations (Eqn.(11)), contain the coupling strength parameters, the second terms of the above equations are just the propagator for excited nucleons. The third terms represent the common multiparticle production amplitudes along with extraneous production modes and the last terms indicate simply the phase space integration terms on the probability of generation of a single π^+ . These expressions are to be calculated by the typical field-theoretical techniques and are to be expressed – if and when necessary – in terms of the relevant variable and/or measured observables.

In order to arrive at the transverse momentum distribution of π^+ , one has to consider the Eqn. (1), eqn. (8) along with eqn. (11). For excess π^+ production, a factor represented by $(1 + \gamma^{\pi^+} p_T^{\pi^+})$ is to be operated on $\frac{1}{2\pi p_T} \frac{d^2 N}{dp_T dy}|_{Cu+Cu \rightarrow \pi^+ X}$ as a multiplier [5]. $\gamma^{\pi^+} \simeq (20\pi g_{p\pi\pi}^2 / \langle n_\pi \rangle) / \sqrt{s} \simeq 0.44$ [1], [11]. Taking $\langle p_T \rangle_{\pi^+} \simeq 0.31$ GeV/c [20], the calculated values of α_{π^+} , $N_R^{\pi^+}$ and β_{π^+} for different centralities and for different energies are given in Table 2. In Figures 3(a), 3(b) and 3(c), we have plotted experimental versus theoretical results for π^+ production in $Cu + Cu$ collisions at energies $\sqrt{s_{NN}} = 22.5, 62.4$ and 200 GeV, respectively. Data are taken from the Refs. [18] and [19]. The solid lines in those Figures are the SCM-based plots.

3.2.2 Production of Positive K-mesons in $Cu + Cu$ Collisions

For the excess production of K^+ -mesons we proceed in the same path as we did earlier for the case of π^+ production. The equation for the extraneous production of K^+ is given hereunder

$$(B_{K^+})_{pp} = \frac{1}{2} (4\pi g_{KN\Lambda}^2 + 4\pi g_{\Sigma KN}^2) \frac{1}{[(P' + K)^2 - m_p^2]^2} A(\nu, q^2)_K \int \frac{d^3 k_K}{2k_0(2\pi)^3} \exp(-ik_K x), \quad (12)$$

Adopting the above procedure, as we indicated for the production of positive pions, we obtain for the transverse momentum distribution of K^+ a multiplicative factor $\sim (1 + \gamma^{K^+} p_T^{K^+})$ to be operated on $\frac{1}{2\pi p_T} \frac{d^2 N}{dp_T dy}|_{Cu+Cu \rightarrow K^+ X}$ [5]. For the production of K^+ , the factor, calculated from eqn.(12), $\gamma^{K^+} \simeq (4\pi g_{KN\Lambda}^2 + 4\pi g_{\Sigma KN}^2) / 2\sqrt{s} \simeq 0.082$ [1], [11]. We use the value of $\langle p_T \rangle_{K^+} \simeq 0.36$ GeV/c [20] and the corresponding values of α_{K^+} , $N_R^{K^+}$ and β_{K^+} for different energies are presented in the Table 3. The experimental results [18], [19] for the production of K^+ of different

centralities and for different energies are plotted in Figures 5(a), 5(b) and 5(c). The solid lines in those figures show the theoretical plots.

3.2.3 Production of Excess Protons

Similarly, for the excess production of protons, the extraneous term can be picked up from our previous work [5] in the following form:

$$(B_p)_{pp} = \frac{4\pi g_{NN\pi}^2}{[(P' + K)^2 - m_p^2]^2} A(\nu, q^2)_{p_s} \int \frac{d^3k_p}{2(2\pi)^3} \exp(-ik_p x), \quad (13)$$

For the production of protons, we obtain for the transverse momentum distribution of p by operating a multiplicative factor $\sim (1 + \gamma^p p_T^p)$, which is an outcome of eqn. (13), on $\frac{1}{2\pi p_T} \frac{d^2N}{dp_T dy}$. The value of $\gamma^p \sim 0.32$ [1] and by taking $\langle p_T \rangle_p \simeq 0.50$ GeV/c [20], we finally obtain the values of α_p , N_R^p and β_p , which are given in the Table 4. In Figures 7(a), 7(b) and 7(c), we have presented the experimental values of invariant yields for proton-production versus the theoretical SCM-based results for energies $\sqrt{s_{NN}} = 22.5, 62.4$ and 200 GeV respectively. Data are taken from [18] and [19]. The lines in the figures show the theoretical outcomes.

3.3 The Ratio Behaviours for Different Secondaries

3.3.1 The π^-/π^+ Ratios at $\sqrt{s_{NN}} = 62.4$ and 200 GeV

The model-based π^-/π^+ ratios for different participating nucleons N_{part} at energies $\sqrt{s_{NN}} = 62.4$ and 200 GeV have been obtained from the expression (8) and Table 2. Data in Figs. 8(a) and 8(b), shown by filled squares and blank circles respectively, are taken from the PHOBOS group [21], [22]. The theoretical values in this regard are plotted by solid line in Figure 8(a) and by filled circles in 8(b).

3.3.2 The K^-/K^+ Ratios at $\sqrt{s_{NN}} = 62.4$ and 200 GeV

In a similar way, the N_{part} versus K^-/K^+ at $\sqrt{s_{NN}} = 62.4$ and 200 GeV can be obtained from equation (8) and Table 3. The calculated values of K^-/K^+ against the N_{part} in the light of SCM are shown by solid line in Fig. 9(a) at energy $\sqrt{s_{NN}} = 62.4$ GeV and by solid squares in Fig. 9(b) at $\sqrt{s_{NN}} = 200$ GeV. The data in those figures are taken from PHOBOS [21], [22].

3.3.3 Some Other Ratio-Behaviours at $\sqrt{s_{NN}} = 62.4$ and 200 GeV

Based on the SCM, the \bar{p}/p ratios at different energies like $\sqrt{s_{NN}} = 62.4$ and 200 GeV and for different participating nucleons N_{part} are obtained with the help of equation (8) and Table 4. The calculated values are plotted in Figs. 10(a) and 10(b) at energies $\sqrt{s_{NN}} = 62.4$ and 200 GeV by solid line and filled circles respectively. Data in those figures are taken from PHOBOS [21], [22].

3.3.4 The \bar{p}/π^- and p/π^+ Ratios at $\sqrt{s_{NN}} = 22.5, 62.4$ and 200 GeV

The expressions for \bar{p}/π^- ratios against p_T for central reactions at energies $\sqrt{s_{NN}} = 22.5, 62.4$ and 200 GeV can be obtained from equation (1) and Table 2 and Table 4 and they are given hereunder

$$\frac{\bar{p}}{\pi^-} = 0.32p_T^{2.038} \exp(-0.15p_T^2) \quad \text{for } \sqrt{s_{NN}} = 22.5 \text{ GeV}, \quad (14)$$

$$\frac{\bar{p}}{\pi^-} = 0.28p_T^{1.932} \exp(-0.15p_T^2) \quad \text{for } \sqrt{s_{NN}} = 62.4 \text{ GeV}, \quad (15)$$

$$\frac{\bar{p}}{\pi^-} = 0.22p_T^{1.821} \exp(-0.13p_T^2) \quad \text{for } \sqrt{s_{NN}} = 200 \text{ GeV}. \quad (16)$$

And for p/π^+ ratios versus p_T at energies $\sqrt{s_{NN}} = 22.5, 62.4$ and 200 GeV the SCM-based equations are written as

$$\frac{p}{\pi^+} = 0.85p_T^{2.038} \exp(-0.15p_T^2) \quad \text{for } \sqrt{s_{NN}} = 22.5 \text{ GeV}, \quad (17)$$

$$\frac{p}{\pi^+} = 0.42p_T^{1.932} \exp(-0.15p_T^2) \quad \text{for } \sqrt{s_{NN}} = 62.4 \text{ GeV}, \quad (18)$$

$$\frac{p}{\pi^+} = 0.35p_T^{1.821} \exp(-0.13p_T^2) \quad \text{for } \sqrt{s_{NN}} = 200 \text{ GeV}. \quad (19)$$

In Figures 11(a) and 11(b) we have plotted p_T versus \bar{p}/π^- and p/π^+ respectively for central $Cu + Cu$ collisions at $\sqrt{s_{NN}} = 22.5, 62.4$ and 200 GeV. Data of these figures are taken from PHENIX [23]. Lines in Figures 11(a) and 11(b) represent eqn. (14)- eqn. (16) and eqn. (17) to eqn. (19) respectively.

3.4 Nuclear Modification Factors

In this subsection we would dwell upon the Nuclear Modification Factors of two types viz., R_{AA} and R_{CP} . In 3.4.1 the former (R_{AA}) would be defined and the results would be hinted, though the figures for both would be shown in the next section. And in 3.4.2 the second one (R_{CP}) would be treated in some detail.

3.4.1 The Nuclear Modification Factor, R_{AA}

The nuclear modification factor (NMF), designated as R_{AA} , for any secondary C , is defined by [23]

$$R_{AA}^C = \frac{(1/N_{AA}^{evt})d^2N_{AA}^C/dp_T dy}{\langle N_{coll}(b) \rangle / \sigma_{pp}^{inel} \times d^2\sigma_{pp}^C/dp_T dy}. \quad (20)$$

Depending on this definition, the SCM-based results on NMFs for $Cu + Cu$ collisions at $\sqrt{s_{NN}} = 22.5, 62.4$ and 200 GeV are deduced on the basis of Eqn.(8), Table 1 and Table 2 and they are given by the undernoted relations

$$R_{AA} = 0.730p_T^{0.621} \quad for \quad \sqrt{s_{NN}} = 22.5 \text{ GeV}, \quad (21)$$

$$R_{AA} = 0.680p_T^{0.311} \quad for \quad \sqrt{s_{NN}} = 62.4 \text{ GeV}, \quad (22)$$

$$R_{AA} = 0.315p_T^{0.234} \quad for \quad \sqrt{s_{NN}} = 200 \text{ GeV}. \quad (23)$$

wherein the values of $\langle N_{coll}(b) \rangle$ to be used are $\approx 140.7, 152.3$ and 182.7 [17] for $Cu + Cu$ collisions at $\sqrt{s_{NN}} = 22.5, 62.4$ and 200 GeV respectively. For N^{evt} , we use the values $\approx 5.8 \times 10^6, 192 \times 10^6$ and 794×10^6 [17] at three different energies and σ_{pp} to be used as 30 mb [24]. Our model-based plot is shown in a figure in the next section.

3.4.2 The Nuclear Modification Factor, R_{CP}

There is yet another nuclear modification factor, R_{CP} which reflects precisely the hadron p_T spectra in different centrality bins and presents comparison of the p_T -spectra between a collision at a specific centrality and the one at the relatively peripheral collision. It is quantified as

$$R_{CP} = \frac{[d^2N/(2\pi p_T dp_T dy)/N_{bin}]^{central}}{[d^2N/(2\pi p_T dp_T dy)/N_{bin}]^{peripheral}}. \quad (24)$$

According to above definition, with the centrality set at $0-10\%$ and the peripherality at $60-94\%$, our model-based expression for R_{CP} in case of neutral pions (π^0 s) is given by

$$R_{CP}^{\pi^0} = 0.543p_T^{-0.054}. \quad (25)$$

wherein we have made use of the values shown in Table-2. The R_{CP} for neutral kaons (K^0 s) with the same centrality and the peripherality changed to $40-60\%$, our model-based result is

$$R_{CP}^{K^0} = 0.664p_T^{-0.235}. \quad (26)$$

wherein we have taken $K^0 = 1/2(K^+ + K^-)$, and used the necessary values from Table-3.

Our model-dependent plots on these two particular observables, R_{AA} and R_{CP} , are shown in the subsequent section on comparative studies.

4 Data and Results on Some Select Observables: A Comparison between Models

We strongly uphold the view that point-to-point or secondary-to-secondary specific comparisons between our model-based results with both data and the other model-based calculations would be quite meaningful and physically significant. But the main and major constraint in this attempt is the lack of availability of such comprehensive calculations encompassing all the light secondaries. In so far as $Cu+Cu$ collisions are concerned, we have, so far, come across two model-based studies, of which one is the application of the Quark Combination Model (QCM) made by Fei et al. [27] for the production of neutral pion/kaon and the other is the pQCD-oriented theoretical study done by Vitev [28] for production of only the neutral pion and for no other secondary. This constitutes a gross limitation to the successful completion of the comparison-aspects in the present study. However, we have tried here to show some comparison(s) only for one or two observables related to a few selected neutral secondaries, with whatever little other model-dependent studies could be obtained upto now.

In spite of the difficulties mentioned in the above paragraph, in the adjoining Fig.12 we compare the data-versus-results based on two models for production of (a) neutral pion and (b) neutral kaon in $Cu + Cu$ collision at $\sqrt{s_{NN}} = 200$ GeV. The standard variety of models that are reckoned with here for comparison with the present SCM are (i) The Quark Combination Model (QCM) and (ii) Perturbative QCD-inspired Vitev's Model. In the former (QCM), the main idea is to line up the quarks and antiquarks in a one-dimensional order in phase space, e.g. in rapidity and let them combine into initial hadrons one by one following a combination rule [27]. These initial hadrons through combination of constituent quarks are then allowed to decay into the final state hadrons through the decay program of PYTHIA 6.1. The calculational steps, in this model, proceed on the basis of two-prong assumptions of two-component model (based on 'soft'-'hard' artifact) and the concept of parton-hadron duality.

The latter model used by us for comparison is one of Vitev [28]. This is essentially a pQCD-oriented model with an analytic model of jet-quenching which embraces medium-induced energy loss after hard partonic scattering. This approach reduces the jet cross-section in the presence of the medium but leaves the parton fragmentation function unaltered. In fact, this feature was conveniently implemented in the analytic model of Vitev [28] for QGP-induced leading hadron suppression. Vitev actually made use of a Hagedornian form of power law expressions

for invariant cross-section(s) and inducted also the radiative energy-loss formalism.

In Fig. (12), the invariant yields versus p_T (GeV/c) for (a) π^0 and (b) K_S^0 for different centralities in $Cu + Cu$ collision at $\sqrt{s_{NN}} = 200$ GeV have been plotted. Data are taken from [29] and [30]. The solid lines in those Figures represent the SCM-based calculations wherein the dashed lines show the QCM-oriented results [27]. And the dotted line in Fig. 12(a) shows pQCD-inspired calculations done by Vitev [28] for production of only the neutral pions in $Cu + Cu$ collision.

4.1 The Nuclear Modification Factor, R_{AA}

In Fig. 13, we plot R_{AA} vs. p_T at energies (a) $\sqrt{s_{NN}} = 22.5$ GeV, (b) $\sqrt{s_{NN}} = 62.4$ GeV and (c) $\sqrt{s_{NN}} = 200$ GeV. The solid lines in the figures show the SCM-based results, wherein the experimental results are taken from Refs. [23], [25] and [26]. The dotted lines in the figures represent the pQCD-based calculations [17],[28]. Moreover, in Fig. 13(d) we have plotted the $\langle R_{AA} \rangle$ vs. N_{part} between the range $2.5 < p_T < 3.5$ GeV/c for the same collision and at the stated energies. Data-points are taken from the experiments by PHENIX Collaboration [17]. The solid lines in the Fig.13(d) represent the our calculationl results and the dashed lines show the corresponding pQCD-oriented theoretical calculations made by Vitev [17],[28].

4.2 The Nuclear Modification Factor, R_{CP}

In Fig. 14(a) we have plotted R_{CP} for the centralities 0 – 10% and 60 – 94% against p_T for the π^0 . The solid line in that Figure represents the SCM-predicted results arising out of the eqn.(25) and the dotted line in that gives the prediction from Quark Combination Model [27]. No data on R_{CP} for production of neutral pions at RHIC energies have yet been reported.

Similarly, in Fig. 14 (b) we have plotted R_{CP} for the centralities 0 – 10% and 40 – 60% against p_T for the K^0 . The solid line in the Figure 14(b) depicts the SCM-based plot against the experimental result [30] while the dotted line in the same figure represents the results attained by the Quark Combination Model [27].

5 Concluding Remarks

The model applied here gives fair description of the p_T -spectra of all the light secondaries with the chosen values of the two parameters. Besides, the centrality-dependence of the p_T -spectra

is also well-reproduced as is indicated by the figures. Slight disagreements observed at very low- p_T ($p_T \ll 1$ GeV/c) are due to the fact that the model has turned effectively into a mixed one with the entry of a power-law form due to the physics of partonic rearrangement factor. This dominance of power-law form disturbs, to a considerable extent, the agreement between data and model-based calculations for the extremely ‘soft’ (very low- p_T) values. Among the secondaries produced, the particle-antiparticle ratios and the proton-pion ratios are also in good agreement with the measured values. The obtained nuclear modification factors represented by R_{AA} and R_{CP} (central-to-peripheral) are also in accord with the measurements. It is to be noted that we achieve all these with a new mechanism and introduction of some simple and basic ansatz like, the physics of large- p_T nucleus-nucleus collisions and by introducing the properties of factorization, scale-breaking, mixed models with the combine of power-and-exponential laws, along with the principles of structural rearrangement factors at large transverse momenta.

Selected comparisons of our model-based results with two other model-dependent calculations reveal neither sharp disagreement with any of them, nor very splendid agreement with either of them which are generically of standard model variety. Rather, on an overall basis, our results are in better agreement with data than either of them. This is a factor which is of some substance and importance to us.

From a careful scrutiny of the fit-parameters we discover the following properties of them: (i) the structural rearrangement factor is clearly centrality dependent; it increases very slowly with gradual rise in the peripherality of the collisions. (ii) Secondly, the coefficients of the p_T^2 in the exponential term are clearly energy-dependent in nature; on the contrary they manifest themselves to be independent of the centrality-measure of the interactions.

The so-called suppression of the cross-sections at large- p_T in heavy ion collisions is addressed here without resorting to the ideas of the ‘jet-quenching’ which is perceived to be to be one of the main conceptual pillars of heavy ion physics.

An interesting question crops up in this connection. Here, we dealt with some aspects of $Cu + Cu$ collisions at RHIC energies. We have chosen to remain silent about the physics of ‘quark-gluon plasma’ (QGP) formation. The perturbative quantum chromodynamics (pQCD) predicted the formation of quark-gluon plasma (QGP). But the RHIC experiments failed to detect any plasma state; rather they found a “new kind of fluid state with very low viscosity”. So QCD prediction faltered at the first pillar. Secondly, how perfect the fluid observed at RHIC is cannot still be ascertained; the answer is not yet without caveats. Thirdly, we do not consider

this proposed ‘plasma’-state to be any startling revelation, because when heated to very high temperatures, caused by the thermal motion of the molecules in the macroscopic matter, the solid substances melt down and turn into a variety of liquid. Almost in a similar manner, if microscopic particle-constituent matter is raised to very high temperatures attained by the extremely energetic collisions, the microscopic matter might also be converted to a liquid of somewhat unknown nature, and thus obviously to a ‘new’ kind [31]-[33]. So we do not pay much attention to the pQCD-based predictions on QGP and /or of suppression phenomena.

Finally, we sum up by stating that (i) the model under consideration here explains and accommodates quite well the data on $Cu + Cu$ collisions at various energies; and (ii) Quite agreeably, the values of R_{CP} obtained by the present calculations are not in good agreement with data. This could be attributed to our neglect of the effects of final state re-scatterings and some other complex physical factors.

Acknowledgements

The authors would like to express their thankful gratitude to the learned Referee for his/her valuable remarks and constructive suggestions in improving the earlier draft of the manuscript.

Table 2: Values of α , N_R and β for π^- and π^+ productions in $Cu + Cu$ collisions at $\sqrt{s_{NN}}=22.5$, 62.4 and 200 GeV

Centrality	$\sqrt{s_{NN}}=22.5$ GeV					
	π^-			π^+		
	α_{π^-}	$N_R^{\pi^-}$	β_{π^-}	α_{π^+}	$N_R^{\pi^+}$	β_{π^+}
0-10%	0.901	3.454	0.703	1.001	3.454	0.703
10-30%	0.492	3.444	0.703	0.572	3.444	0.703
30-60%	0.239	3.413	0.703	0.244	3.413	0.703
60-100%	0.033	3.410	0.703	0.034	3.410	0.703
Minbias	0.395	3.431	0.703	0.468	3.431	0.703
Centrality	$\sqrt{s_{NN}}=62.4$ GeV					
	π^-			π^+		
	α_{π^-}	$N_R^{\pi^-}$	β_{π^-}	α_{π^+}	$N_R^{\pi^+}$	β_{π^+}
0-10%	0.707	3.035	0.468	0.786	3.035	0.468
10-30%	0.464	3.030	0.468	0.474	3.030	0.468
30-60%	0.180	3.026	0.468	0.228	3.026	0.468
60-100%	0.038	3.016	0.468	0.044	3.016	0.468
Minbias	0.204	3.142	0.468	0.207	3.142	0.468
Centrality	$\sqrt{s_{NN}}=200$ GeV					
	π^-			π^+		
	α_{π^-}	$N_R^{\pi^-}$	β_{π^-}	α_{π^+}	$N_R^{\pi^+}$	β_{π^+}
0-5%	1.098	3.597	0.293	1.113	3.597	0.293
5-10%	0.898	3.572	0.293	0.910	3.572	0.293
10-15%	0.750	3.567	0.293	0.760	3.567	0.293
15-20%	0.687	3.552	0.293	0.696	3.552	0.293
20-30%	0.635	3.544	0.293	0.643	3.544	0.293
30-40%	0.523	3.525	0.293	0.530	3.525	0.293
40-50%	0.353	3.518	0.293	0.358	3.518	0.293
50-60%	0.283	3.508	0.293	0.287	3.508	0.293
60-70%	0.113	3.491	0.293	0.115	3.491	0.293
70-80%	0.085	3.476	0.293	0.086	3.476	0.293
80-92%	0.004	3.453	0.293	0.004	3.453	0.293

Table 3: Values of α , N_R and β for K^- and K^+ productions in $Cu+Cu$ collisions at $\sqrt{s_{NN}}=22.5$, 62.4 and 200 GeV

Centrality	$\sqrt{s_{NN}}=22.5$ GeV					
	K^-			K^+		
	α_{K^-}	$N_R^{K^-}$	β_{K^-}	α_{K^+}	$N_R^{K^+}$	β_{K^+}
0-10%	0.406	2.304	0.863	0.469	2.304	0.863
10-30%	0.185	2.285	0.863	0.255	2.285	0.863
30-60%	0.069	2.274	0.863	0.114	2.274	0.863
60-100%	0.012	2.270	0.863	0.018	2.270	0.863
Minbias	0.118	2.264	0.863	0.151	2.264	0.863
Centrality	$\sqrt{s_{NN}}=62.4$ GeV					
	K^-			K^+		
	α_{K^-}	$N_R^{K^-}$	β_{K^-}	α_{K^+}	$N_R^{K^+}$	β_{K^+}
0-10%	0.675	2.714	0.571	0.755	2.714	0.571
10-30%	0.405	2.704	0.571	0.524	2.704	0.571
30-60%	0.162	2.688	0.571	0.187	2.688	0.571
60-100%	0.023	2.658	0.571	0.028	2.658	0.571
Minbias	0.217	2.681	0.571	0.251	2.681	0.571
Centrality	$\sqrt{s_{NN}}=200$ GeV					
	K^-			K^+		
	α_{K^-}	$N_R^{K^-}$	β_{K^-}	α_{K^+}	$N_R^{K^+}$	β_{K^+}
0-5%	0.286	2.939	0.417	0.294	2.939	0.417
5-10%	0.250	2.839	0.417	0.257	2.839	0.417
10-15%	0.214	2.819	0.417	0.220	2.819	0.417
15-20%	0.210	2.805	0.417	0.216	2.805	0.417
20-30%	0.181	2.795	0.417	0.186	2.795	0.417
30-40%	0.165	2.765	0.417	0.170	2.765	0.417
40-50%	0.112	2.734	0.417	0.115	2.734	0.417
50-60%	0.051	2.714	0.417	0.053	2.714	0.417
60-70%	0.041	2.698	0.417	0.042	2.698	0.417
70-80%	0.024	2.672	0.417	0.026	2.672	0.417
80-92%	0.013	2.652	0.417	0.014	2.652	0.417

Table 4: Values of α , N_R and β for \bar{p} and p productions in $Cu + Cu$ collisions at $\sqrt{s_{NN}}=22.5$, 62.4 and 200 GeV

Centrality	$\sqrt{s_{NN}}=22.5$ GeV					
	\bar{p}			p		
	$\alpha_{\bar{p}}$	$N_R^{\bar{p}}$	$\beta_{\bar{p}}$	α_p	N_R^p	β_p
0-10%	0.211	0.826	0.853	0.344	0.826	0.853
10-30%	0.111	0.780	0.853	0.129	0.780	0.853
30-60%	0.044	0.695	0.853	0.051	0.695	0.853
60-100%	0.008	0.691	0.853	0.010	0.691	0.853
Minbias	0.070	0.798	0.853	0.101	0.798	0.853
Centrality	$\sqrt{s_{NN}}=62.4$ GeV					
	\bar{p}			p		
	$\alpha_{\bar{p}}$	$N_R^{\bar{p}}$	$\beta_{\bar{p}}$	α_p	N_R^p	β_p
0-10%	0.468	1.118	0.618	0.957	1.118	0.618
10-30%	0.256	0.958	0.618	0.513	0.958	0.618
30-60%	0.108	0.945	0.618	0.192	0.945	0.618
60-100%	0.012	0.930	0.618	0.023	0.930	0.618
Minbias	0.184	1.178	0.618	0.298	1.178	0.618
Centrality	$\sqrt{s_{NN}}=200$ GeV					
	\bar{p}			p		
	$\alpha_{\bar{p}}$	$N_R^{\bar{p}}$	$\beta_{\bar{p}}$	α_p	N_R^p	β_p
0-5%	0.166	1.251	0.426	0.185	1.251	0.426
5-10%	0.156	1.231	0.426	0.181	1.231	0.426
10-15%	0.113	1.211	0.426	0.131	1.211	0.426
15-20%	0.105	1.192	0.426	0.122	1.192	0.426
20-30%	0.087	1.172	0.426	0.101	1.172	0.426
30-40%	0.074	1.154	0.426	0.086	1.154	0.426
40-50%	0.038	1.133	0.426	0.044	1.133	0.426
50-60%	0.028	1.112	0.426	0.032	1.112	0.426
60-70%	0.017	1.105	0.426	0.020	1.105	0.426
70-80%	0.006	1.099	0.426	0.007	1.099	0.426
80-92%	0.003	1.075	0.426	0.004	1.075	0.426

References

- [1] P. Guptaroy, Bhaskar De, G. Sau, S. K. Biswas, S. Bhattacharyya, *Int. J. Mod. Phys. A* **28**,5121 (2007) and the references therein.
- [2] P. Bandyopadhyay and S. Bhattacharyya, *IL Nuovo Cimento A***43**, 305 (1978).
- [3] P. Bandyopadhyay, R. K. Roychoudhury, S. Bhattachayya and D. P. Bhattacharyya, *IL Nuovo Cimento A* **50**, 133 (1979).
- [4] S. Bhattacharyya, *IL Nuovo Cimento C***11**, 51 (1988).
- [5] S. Bhattacharyya, *J. Phys. G***14**, 9 (1988).
- [6] P. Guptaroy, G. Sau, S. K. Biswas, S. Bhattacharyya, *Mod. Phys. Lett. A* **23**, 1031 (2008).
- [7] C. Y. Wong:‘Introduction to High-Energy Heavy Ion Collisions’ (World Scientific,1994).
- [8] K. J. Eskola, P. V. Ruuskanen and K. Tuominen, *Phys. Lett. B* **543**, 208 (2002).
- [9] M.I. Gorenstein, A. P. Kostyuk, H. Stöcker and W. Greiner, *Phys. Lett. B* **524**, 264 (2002).
- [10] NA50 Collaboration: M.C.Abreu et al, Preprint, CERN-EP/2002-017(Feb. 15, 2002).
- [11] P. Guptaroy, B.De, S. Bhattacharyya, D. P. Bhattacharyya, *Int. J. Mod. Phys. E* **12**, 493 (2003).
- [12] D. d’Enterria, *J. Phys. G***31**, s491 (2005).
- [13] B. Alper et al., *Nucl. Phys. B***100**, 237 (1975).
- [14] S. S. Adler et al. (PHENIX Collaboration), *Phys. Rev. C***74**, 024904 (2006). [arXiv:nucl-ex/0603010 V1,(8 Mar 2006)].
- [15] H. Yang for BRAHMS Collaboration, *J. Phys. G***34**, s619 (2007). [arXiv:nucl-ex/0702004 V1,(5 Feb 2007)].
- [16] B. Alver et al., *Phys. Rev. Lett.* **96**, 212301 (2006).
- [17] A. Adare et al. (PHENIX Collaboration), *Phys. Rev. Lett.* **101**, 162301 (2008). [arXiv:0801.4555 V1 [nucl-ex] (29 Jan 2008)].
- [18] T. Chujo, Hot Quarks 2006, <http://www.phenix.bnl.gov/WWW/publish/chujo/presentation>.
- [19] http://www.phenix.bnl.gov/WWW/show_plot.php.html.
- [20] B. Alver et al., *Phys. Rev. C***77**, 061901 (2008). [arXiv:0802.1695[nucl-ex] (1 May 2008)].
- [21] G. I Veres for PHOBOS Collaboration, *J. Phys. G***34**, s1103 (2007).
- [22] B. Wosiek for PHOBOS Collaboration, *J. Phys. G***35**, 104005 (2008). [arXiv:0804.4352V1[nucl-ex] (28 Apr. 2008)].
- [23] T. Chujo for the PHENIX Collaboration, *Eur. Phys. J. C***49**, 23 (2007).
- [24] S. Bhattacharyya, B. De, P. Guptaroy, A. C. Das Ghosh, *Czech. J. Phys.* **52**, 781 (2002).

- [25] T. C. Awes for PHENIX Collaboration, *J. Phys.* **G35**, 104007 (2008)[arXiv:0805.1636 V1 [nucl-ex] (12 May 2008)].
- [26] K. Reygers for PHENIX Collaboration, arXiv:*J. Phys.* **G35**, 104045 (2008) [arXiv:0804.4562 V1 [nucl-ex] (29 Apr. 2008)].
- [27] W.Yun-Fei, S. Feng-Lan, S. Jun, W. De-Ming, X. Qu-Bing, *Chin. Phys.* **C32**, 976 (2008) [arXiv:0802.2579 V2 [hep-ph] (05 Mar. 2009)].
- [28] I. Vitev, *Phys. Lett.* **B639**, 38 (2006).
- [29] T. Sakaguchi, (For the PHENIX Collaboration), *Int. J. Mod. Phys.* **E16**, 2166 (2007) [arXiv:nucl-ex/0703027 (16 May 2007)].
- [30] A. R. Timmins for STAR Collaboration, *Int. J. Mod. Phys.* **E16**, 2055 (2007) [arXiv:0708.3290[nucl-ex](24 Aug. 2007)].
- [31] A. Majumder, B. Müller and X. N. Wang, *Phys. Rev. Lett.***99**, 192301 (2007).
- [32] R. Stock, arXiv:0907.5071v1 [nucl-ex] 29 Jul 2009
- [33] G. Sau, S. K. Biswas, B. De, P. Guptaroy, A. Bhattacharya, S. Bhattacharyya, *Can. J. Phys.*, **87**, 135 (2009).

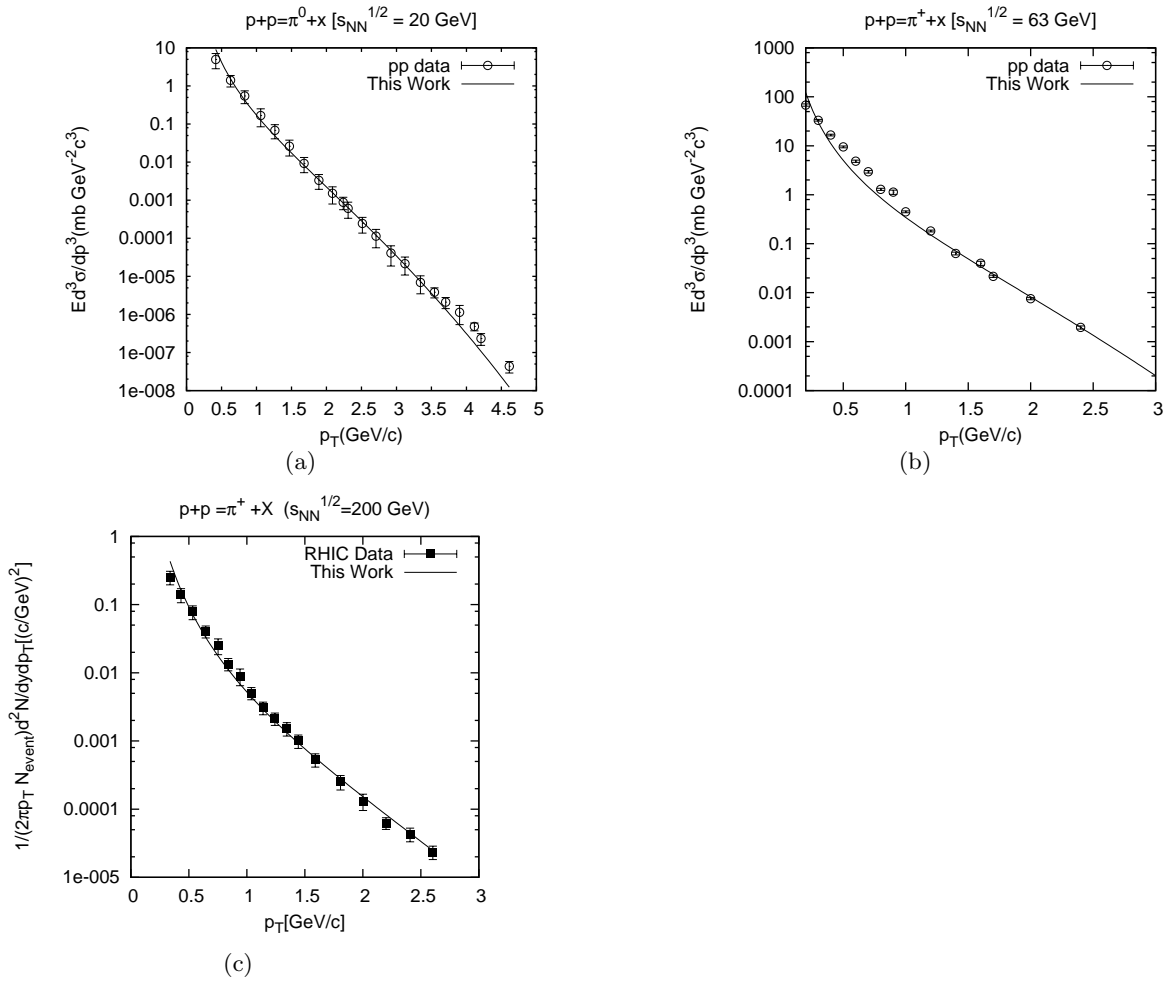


Figure 1: Plots for π production in $p+p$ collisions at energies (a) $\sqrt{s_{NN}} = 20$ GeV, (b) $\sqrt{s_{NN}} = 63$ GeV and (c) $\sqrt{s_{NN}} = 200$ GeV. Data are taken (a) from Ref. [12], (b) from Ref. [19] and (c) from Refs [14], [15]. Solid lines in the Figures show the SCM-based plots.

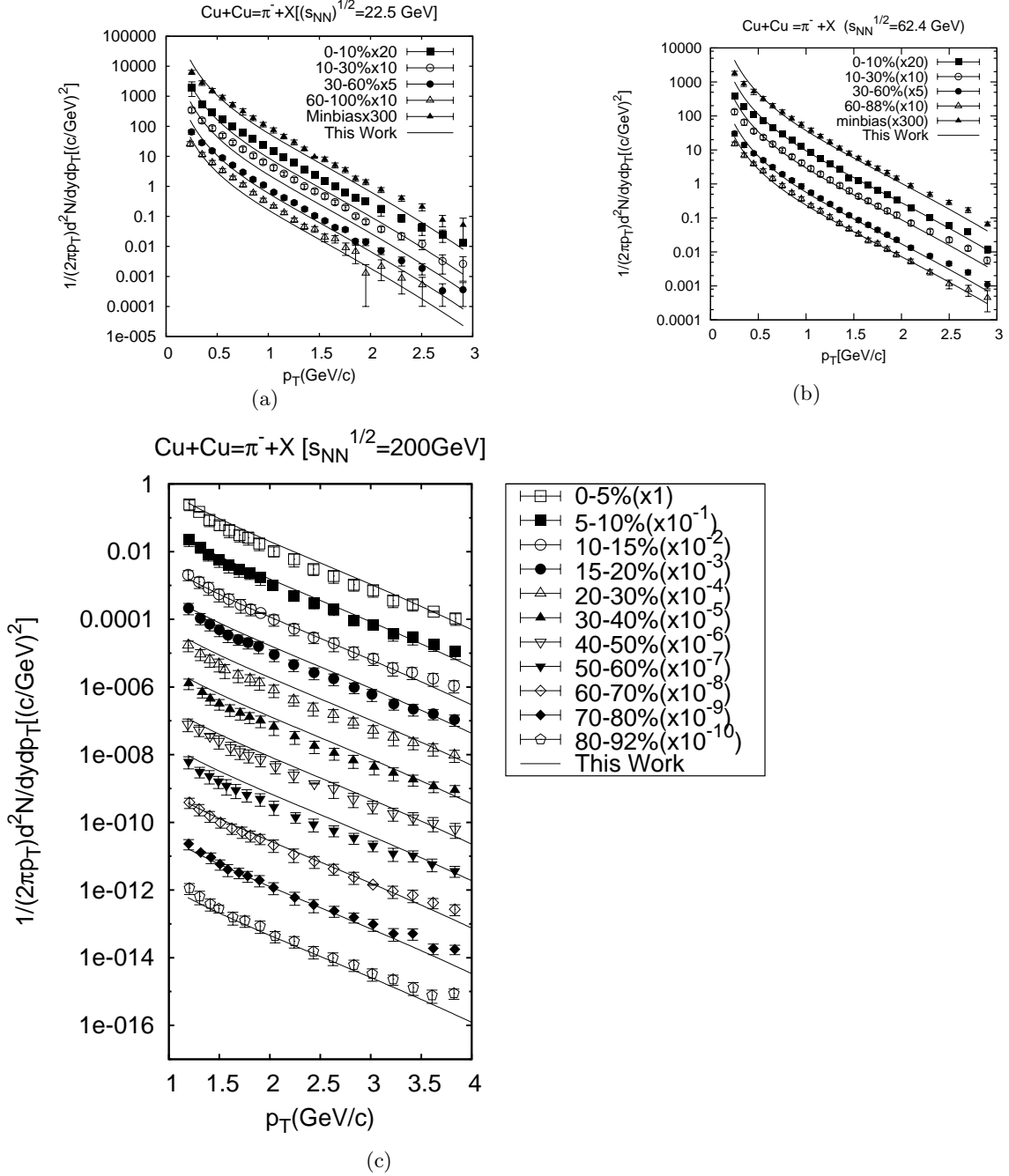


Figure 2: Centrality dependence of the p_T distribution for π^- for different centralities and at energies (a) 22.5 GeV [18], (b) 62.4 GeV [18] and (c) 200 GeV [19] in $Cu + Cu$ collisions. The solid lines in the Figures 2(a), 2(b) and 2(c) show the SCM calculations for different centralities.

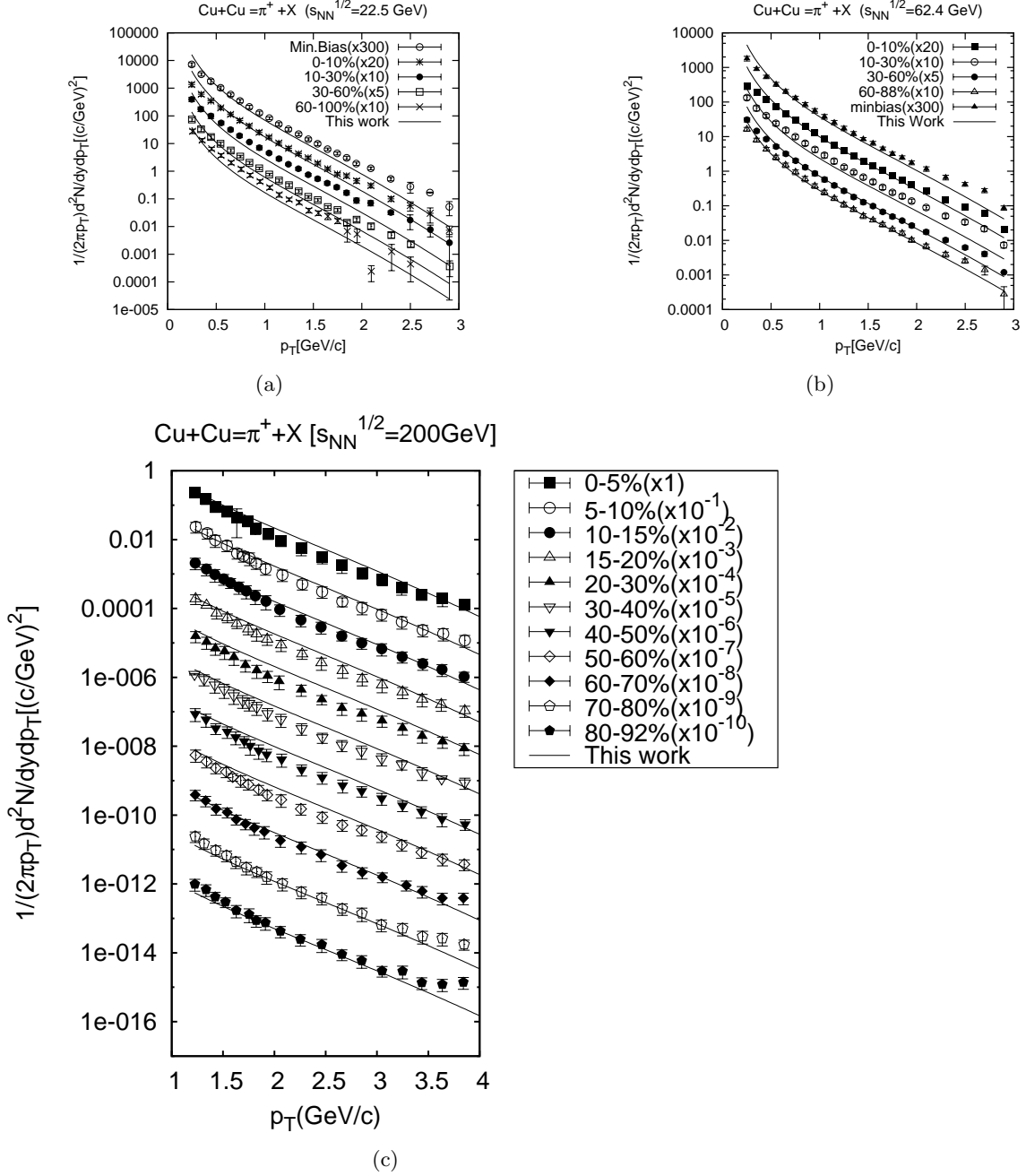


Figure 3: Centrality dependence of the p_T distribution for π^+ for different centralities and at energies (a) 22.5 GeV [18], (b) 62.4 GeV [18] and (c) 200 GeV [19] in $Cu + Cu$ collisions. The solid lines in the Figures 3(a), 3(b) and 3(c) show the SCM calculations for different centralities.

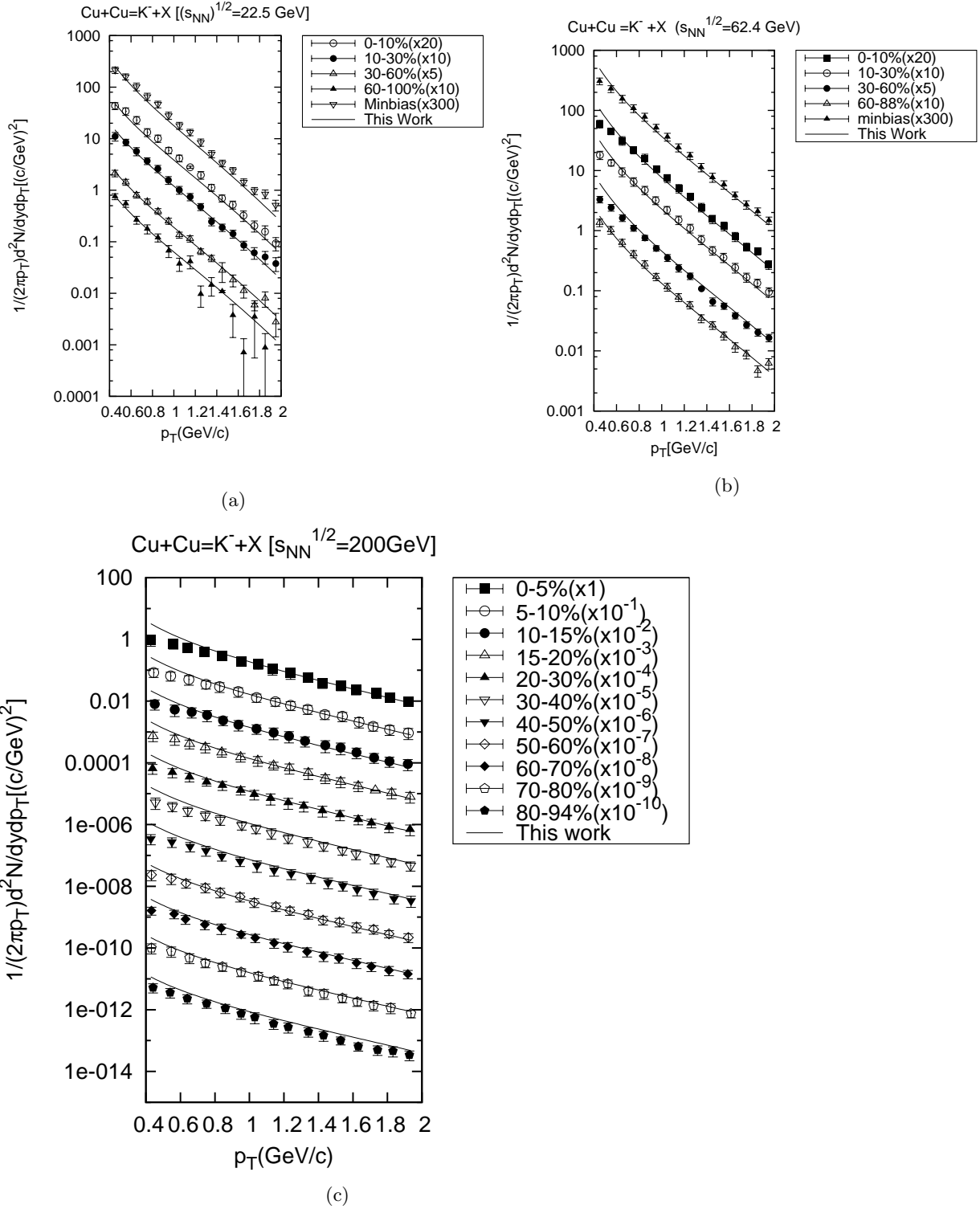


Figure 4: Invariant spectra as function of p_T for K^- production in $Cu + Cu$ collisions at (a) $\sqrt{s_{NN}} = 22.5$ GeV [18], (b) $\sqrt{s_{NN}} = 62.4$ GeV [18] and for (c) $\sqrt{s_{NN}} = 200$ GeV [19]. The solid lines show the SCM-based results.

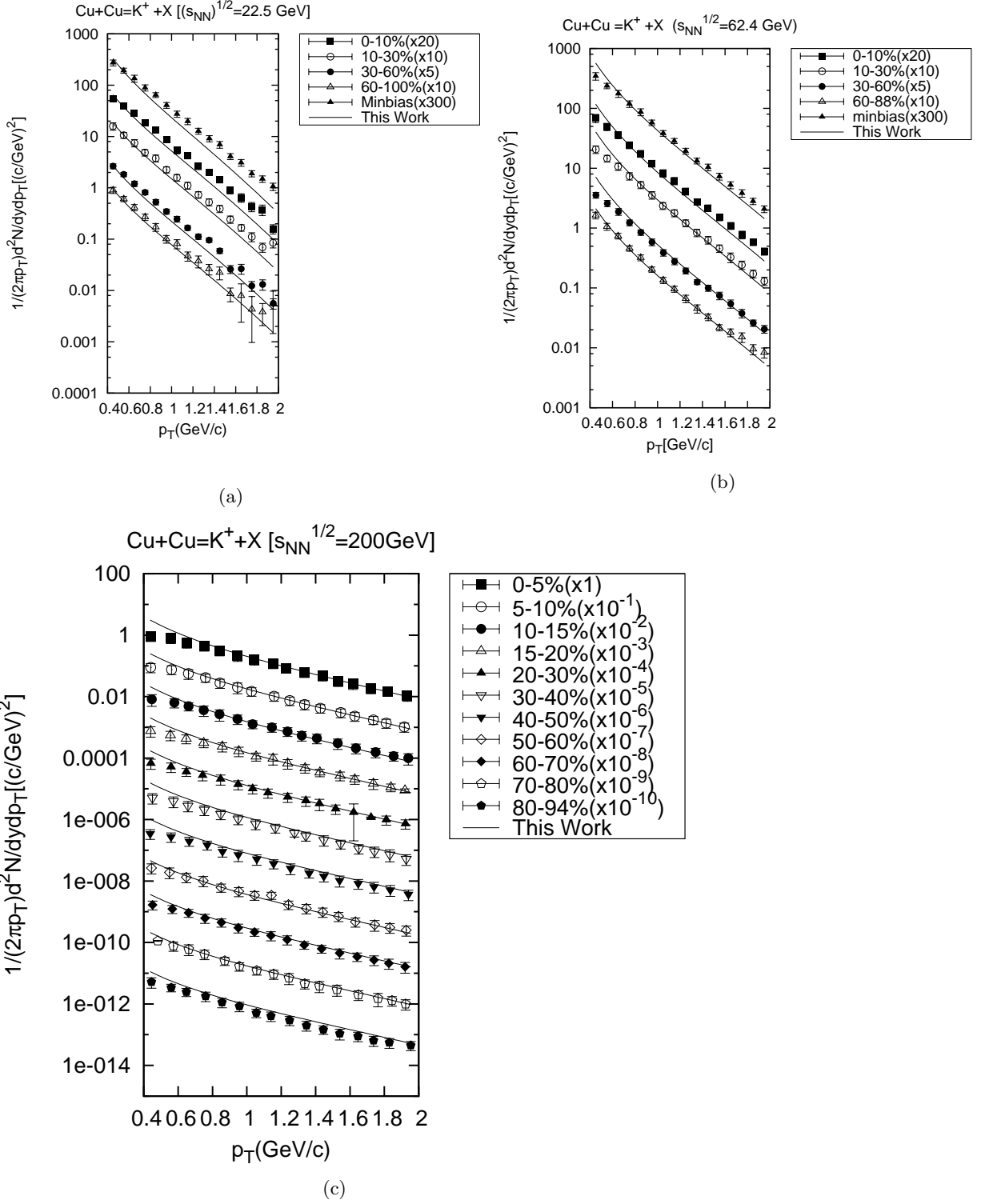


Figure 5: Invariant spectra as function of p_T for K^+ production in $Cu + Cu$ collisions at (a) $\sqrt{s_{NN}} = 22.5$ GeV [18], (b) $\sqrt{s_{NN}} = 62.4$ GeV [18] and for (c) $\sqrt{s_{NN}} = 200$ GeV [19]. The solid lines show the SCM-based results.

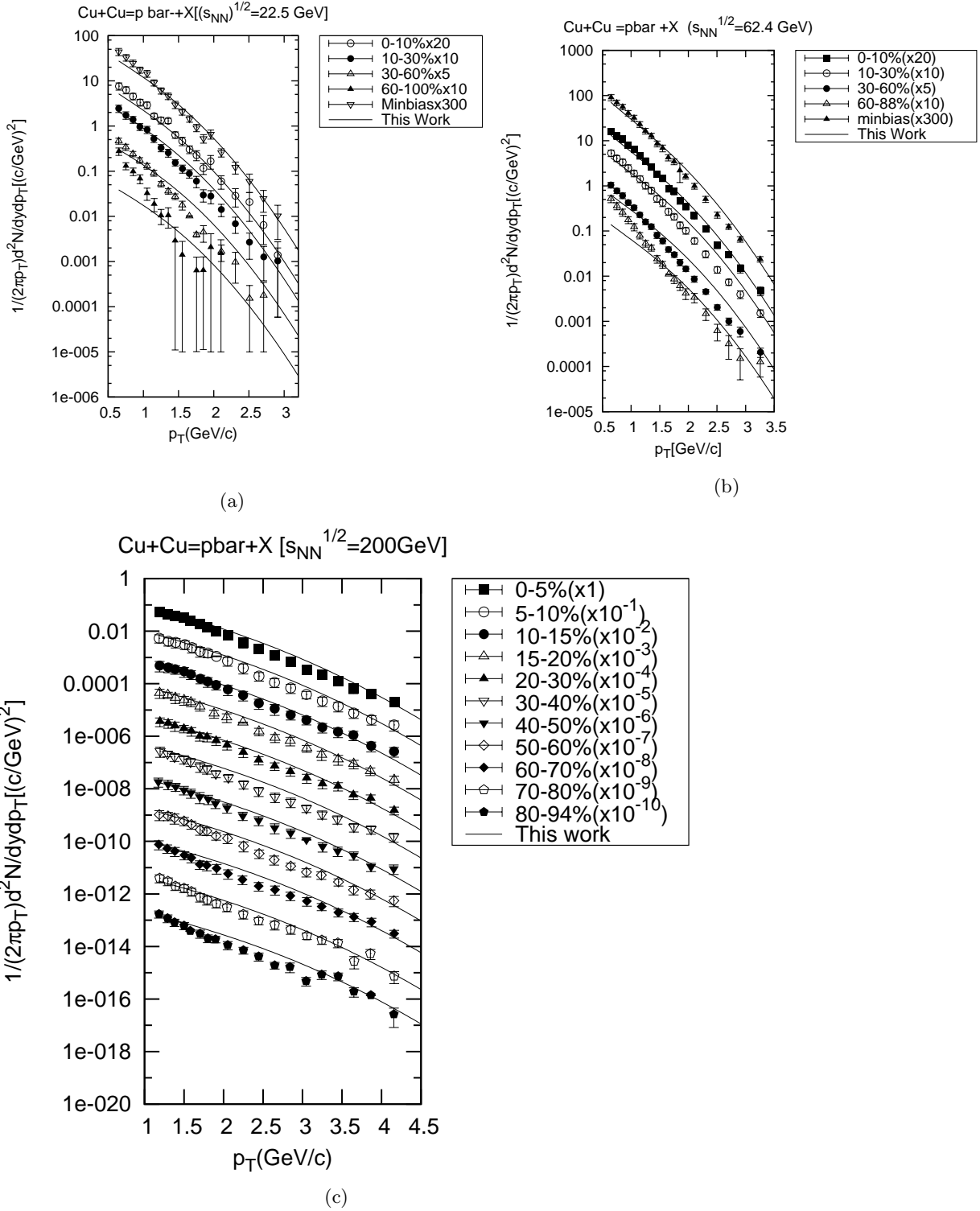


Figure 6: Centrality dependence of the p_T distribution for \bar{p} for different centralities in $Cu+Cu$ collisions at (a) $\sqrt{s_{NN}} = 22.5$ GeV [18], (b) $\sqrt{s_{NN}} = 62.4$ GeV [18] and for (c) $\sqrt{s_{NN}} = 200$ GeV [19]. The solid lines in the Figures show the SCM calculations .

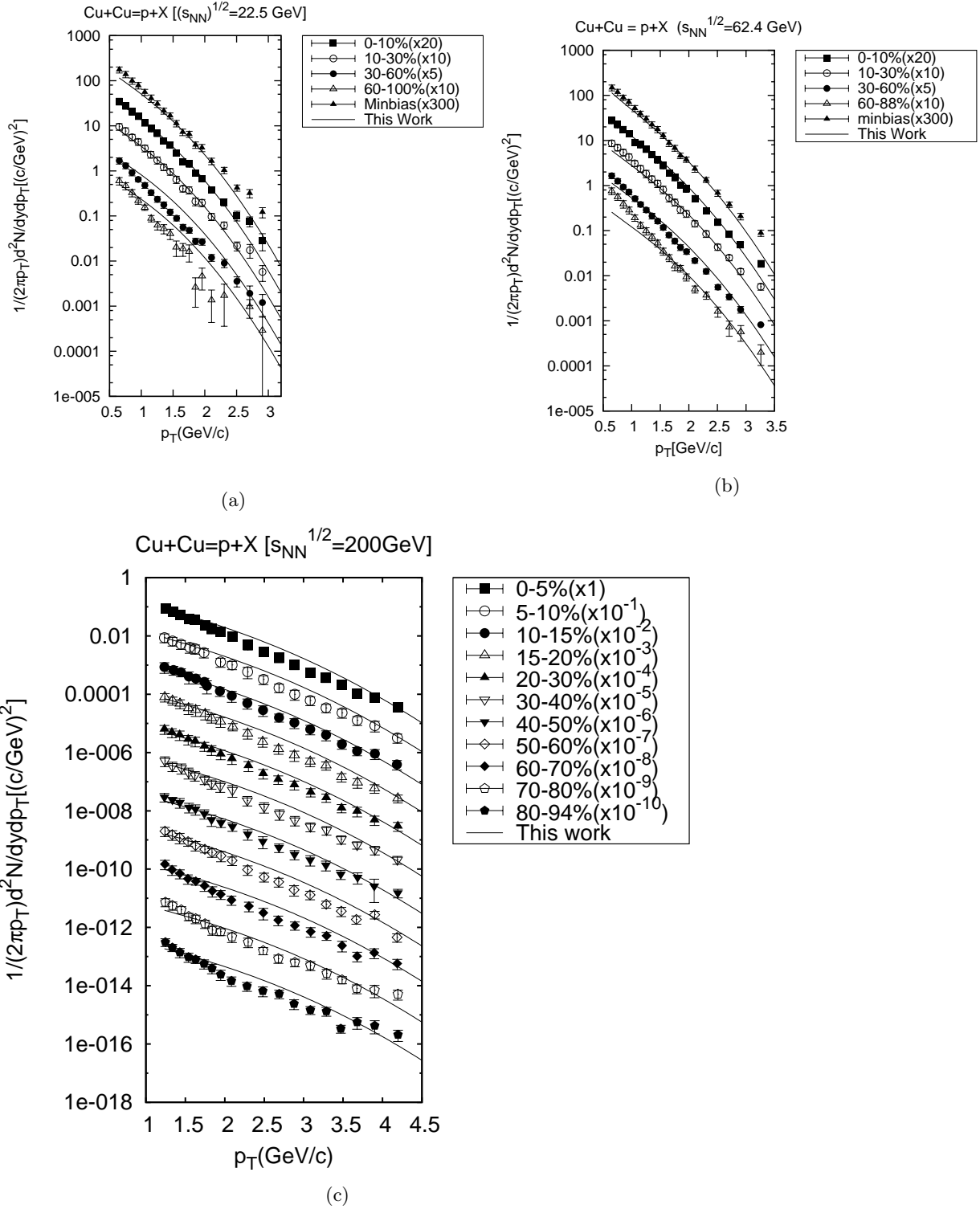


Figure 7: Centrality dependence of the p_T distribution for p for different centralities in $Cu+Cu$ collisions at (a) $\sqrt{s_{NN}} = 22.5$ GeV [18], (b) $\sqrt{s_{NN}} = 62.4$ GeV [18] and for (c) $\sqrt{s_{NN}} = 200$ GeV [19]. The solid lines in the figures show the SCM calculations .

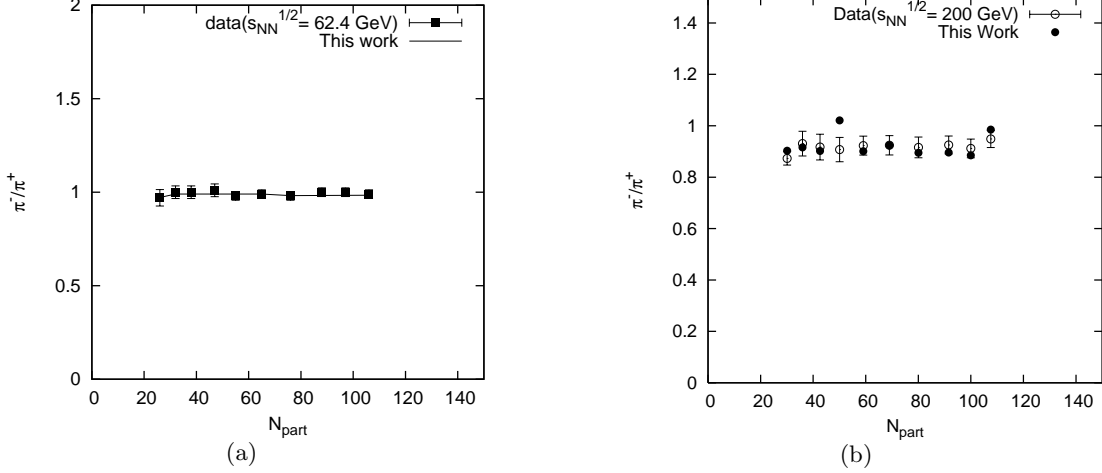


Figure 8: The N_{part} versus π^-/π^+ ratio behaviours at (a) $\sqrt{s_{NN}} = 62.4$ GeV and (b) $\sqrt{s_{NN}} = 200$ GeV. Data are taken from PHOBOS [21], [22]. The solid line in Fig. 8(a) and the filled circles in Fig. 8(b) show the theoretically calculated values.

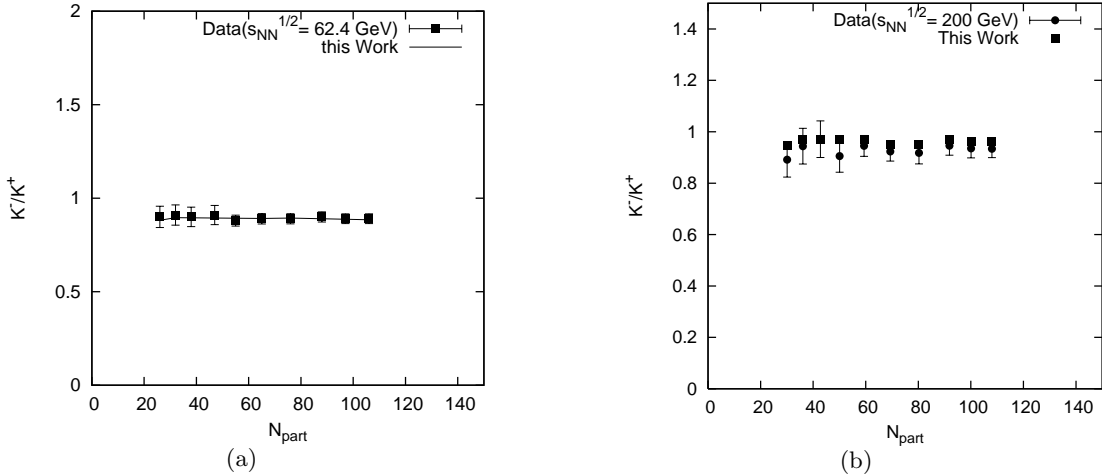


Figure 9: The N_{part} versus K^-/K^+ ratio behaviours at (a) $\sqrt{s_{NN}} = 62.4$ GeV and (b) $\sqrt{s_{NN}} = 200$ GeV. Data are taken from PHOBOS [21], [22]. The solid line in Fig. 9(a) and the filled squares in Fig. 9(b) show the SCM-based calculated values.

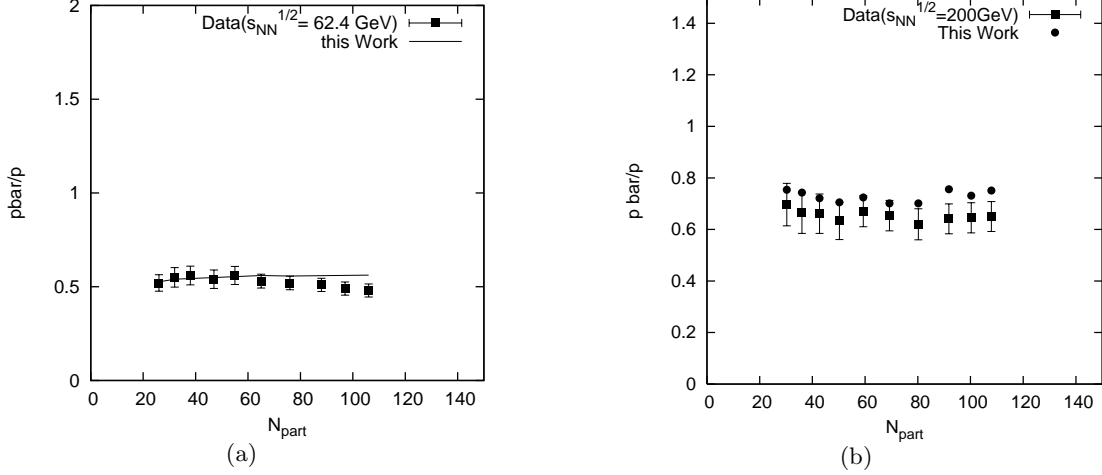


Figure 10: The \bar{p}/p ratio behaviours as a function of number of participants (N_{part}) in $Cu + Cu$ reaction at (a) $\sqrt{s_{NN}} = 62.4$ GeV and (b) at $\sqrt{s_{NN}} = 200$ GeV. Data are taken from PHOBOS [21], [22]. The solid line in Fig. 10(a) and the filled circles in Fig. 10(b) show the SCM-based calculated values.

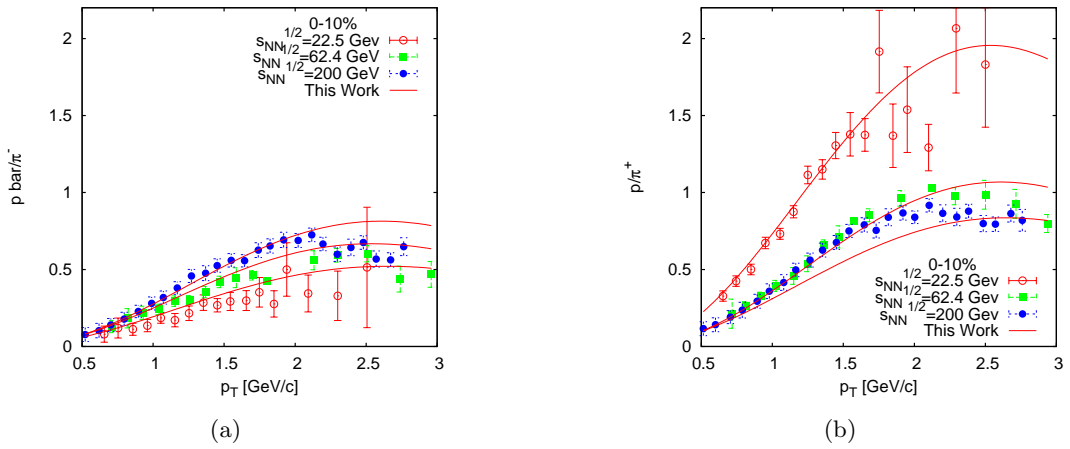


Figure 11: Ratios of (a) \bar{p}/π^- and (b) p/π^+ as a function p_T for central $Cu + Cu$ reactions at $\sqrt{s_{NN}} = 22.5, 62.4$ and 200 GeV. Data in these Figures are taken from [23]. The solid lines show the SCM-based results.

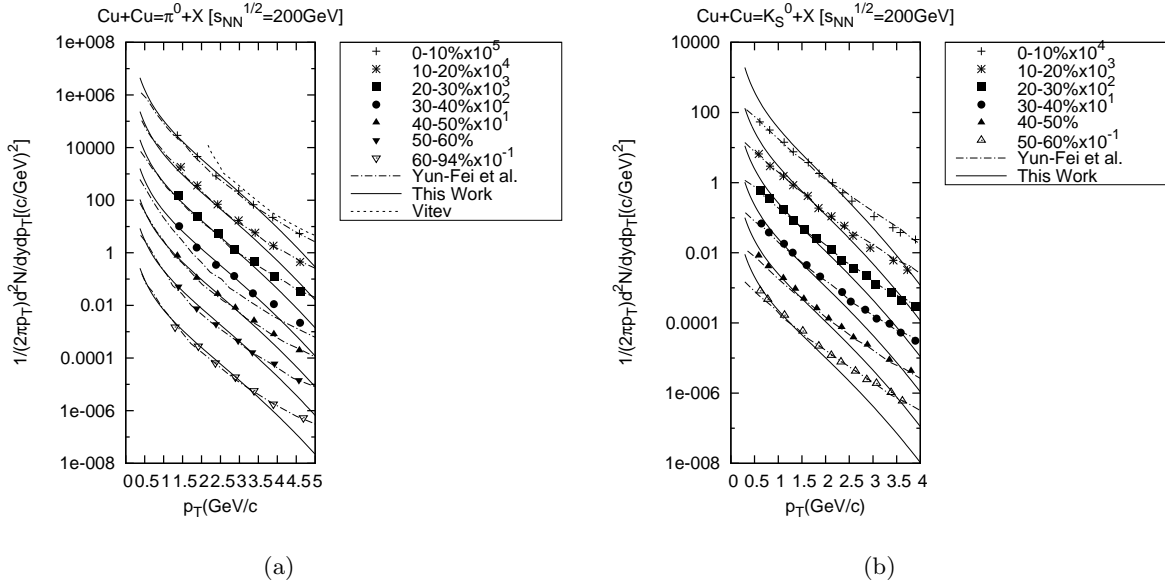


Figure 12: Comparisons (a) between the SCM, the Quark Combination Model [27] and the pQCD approach [28] for the π^0 production at 200 GeV[19] and (b) between the SCM, the Quark Combination Model [27] for the K_S^0 production for $Cu + Cu$ reactions at $\sqrt{s_{NN}} = 200$ GeV. Data are taken from [29] and [30]. The solid lines in those figures represent SCM-based results, wherein the dashed and dotted lines represent the Quark Combination Model [27] and the pQCD approach [28].

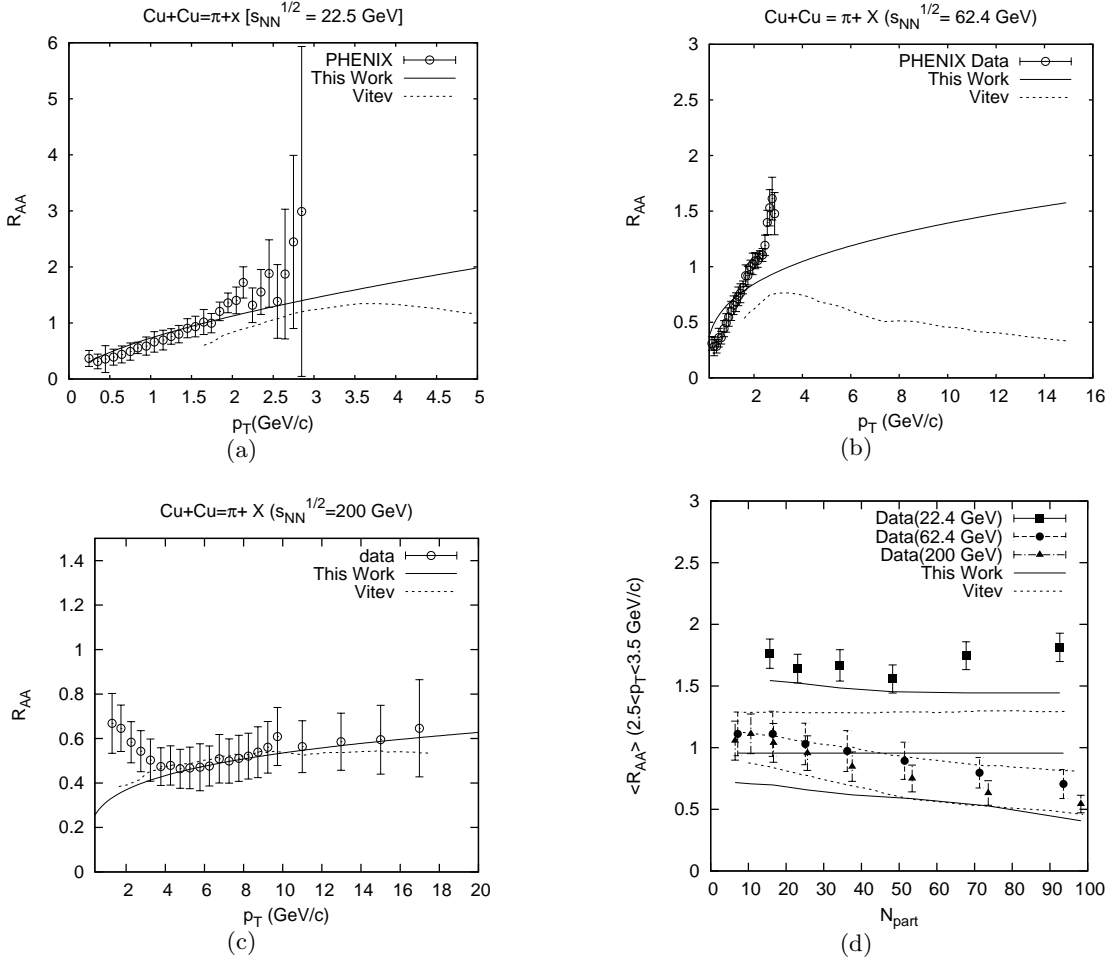


Figure 13: Plots of p_T versus R_{AA} (as defined in the text) at energies (a) $\sqrt{s_{NN}} = 22.5$ GeV, (b) $\sqrt{s_{NN}} = 62.4$ and (c) $\sqrt{s_{NN}} = 200$ GeV. Data in these Figures are from [23], [25] and [26]. The solid lines show the SCM-based results, wherein the dashed lines represent the pQCD-oriented calculations [17],[28]. (d) Plot of $\langle R_{AA} \rangle$ vs. N_{part} for p_T -ranges like $2.5 < p_T < 3.5$ GeV/c. Comparisons of the nature of average nuclear modification factors based on two sets of calculations, one done by SCM and represented by solid lines and the other (dashed lines) obtained and shown by Vitev [17],[28] are made here.

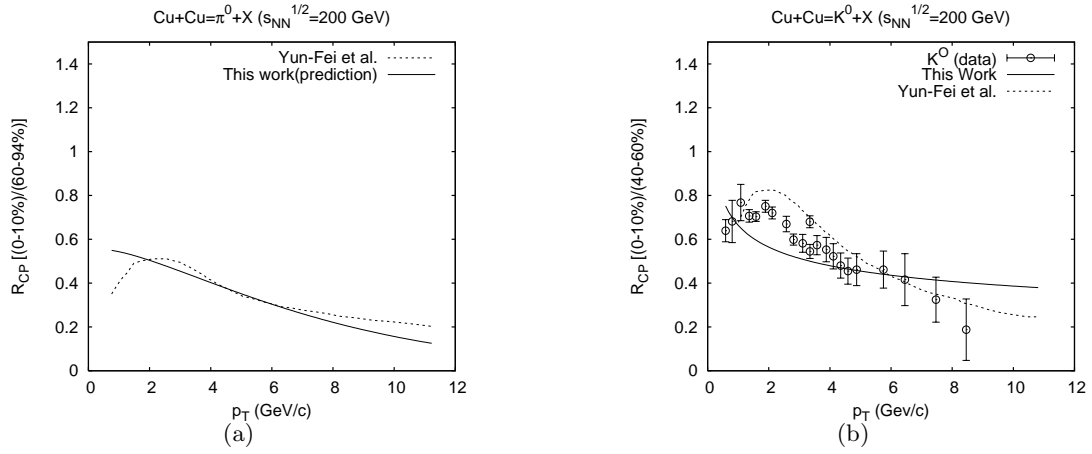


Figure 14: Plots for the R_{CP} behaviours versus p_T of (a) π^0 and (b) K^0 . Pion data for $Cu + Cu$ collisions has not yet available. Plots in Fig.14(a) are predictive comparison between SCM-based result and result from Yun-Fei et al.[27]. Data in Fig. (b) are taken from STAR [30]. The solid line in Fig. 14(b) shows the SCM-based results while the dotted line represents the results of Yun-Fei et al.[27].